MEDWIN PUBLISHERS
Committed to create value for Researchers

International Journal of Oceanography & Aquaculture

Evaluation of the Hf-Radar Network System around Taiwan using Normalized Cumulative Lagrangian Separation

Erick Fredj[1]*, Josh Kohut[2], Hugh Roarty[2] and Jain-Wai Lu[3]

[1]Department of Computer Sciences, Lev Academic Center, Israel

[2]Department of Marine and Coastal Sciences Rutgers, The State University of New Jersey, USA

[3]Taiwan Ocean Research Institute, National Applied Research Laboratories, Taiwan

Research Article

Volume 1 Issue 1

Received Date: January 30, 2017

Published Date: March 22, 2017

***Corresponding author:** Erick Fredj, Department of Computer Sciences, Lev Academic Center, 21 Havaad Haleumi Street PO Box 16031, 91160 Jerusalem, Israel, Tel: +972 2 6751018; E-mail: fredj@jct.ac.il

Abstract

The Lagrangian separation distance between the endpoints of simulated and observed drifter trajectories is often used to assess the performance of numerical particle trajectory models. However, the separation distance fails to indicate relative model performance in weak and strong current regions, such as over continental shelves and the adjacent deep ocean. A skill score described in detail by Lui, et al. was applied to estimate the cumulative Lagrangian separation distances normalized by the associated cumulative trajectory lengths [1]. The proposed dimensionless skill score is particularly useful when the number of drifter trajectories is limited and neither a conventional Eulerian-based velocity nor a Lagrangian based probability density function may be estimated. The skill score assesses The Taiwan Ocean Radar Observing System (TOROS) performance. TOROS consists of 17 SeaSonde type radars around the Taiwan Island. The currents off Taiwan are significantly influenced by the nearby Kuroshio Current. The TOROS High Frequency radars network product is useful for providing essential information on ocean surface currents of use in water property transports, fishing, offshore oil and gas operations, hazardous spill mitigation, search and rescue, etc.

Keywords: Lagrangian Skill Score; Altimetry; Drifter; Hf-Radar

Introduction

Taiwan and its outlying islands' nearly 1,600 kilometers of coastline and 42,000 square kilometers of territorial sea possess rich and diverse coastal features, marine biological resources, and marine ecosystems (Figure 1). The many ecosystems, including coral reefs, wetlands, mangroves, lagoons, algal reefs, estuaries, and beaches/sandbars, provide many forms of "ecosystem services," such as "supporting," "provisioning," "regulating," and "cultural" services, yielding many benefits and products, including fishery resources, coastal protection, water purification, tourism and recreation opportunities. In addition, the fact that Taiwan is surrounded by sea also supports the development of many industries, including shipping, shipbuilding, coastal engineering, offshore wind power, oil and mineral exploration, biotechnology, and so on. The Taiwanese coastal ocean is a complex system that forms the boundary between the land and the deep ocean. Deeper understanding of surface currents can be extremely valuable when one seeks to characterize and quantify the

transport of plankton and anthropogenic material in the coastal ocean [2]. Many observations such as Glider, ADCP, High Frequency Radar and Altimetry, are required to collect data from both deep and coastal ocean. In particular, accurate prediction of the path of a drifting search target given estimates of an initial location and the evolution of the velocity field is a crucial step. Furthermore, the currents off Taiwan are significantly influenced by the nearby Kuroshio current, as demonstrated in the below diagram.

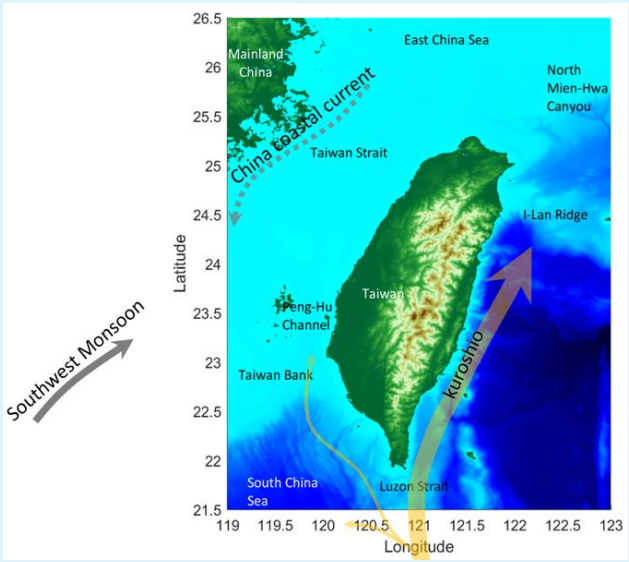

Figure 1: The schematic diagram of near circulation current is shown on a top of the bathymetric chart of areas around Taiwan.

The Kuroshio has two velocity maximum cores southeast of Taiwan, which gradually combine into one as the Kuroshio flowed north. The Kuroshio is deflected by the I-Lan Ridge east of Taiwan and the zonal-running shelf break northeast of Taiwan. At the shelf break, the Kuroshio splits, with one branch intruding onto the shelf. West of the Luzon Strait, the Kuroshio intrudes into the South China Sea. Some water flows northward into the Taiwan Strait and re-joins the Kuroshio. Currents in the Taiwan Strait flow primarily in a northward direction, except for the southward current near the coast of Mainland China. North of the Taiwan Strait, a branch of the northward flow follows the northern coast of Taiwan to join the Kuroshio. The composite current varies consistently from season to season. There is generally poor correlation between currents and local winds, especially in the deep-water regime. Remote forces are important in the currents around Taiwan. The Taiwan Strait (TS), bounded by the mainland to the west and the island of Taiwan to the east, is a narrow passage that connects the East China Sea (ECS) in the north to the South China Sea (SCS) in the south (see Figure 1). The seasonal circulation in the TS, primarily dominated by monsoons and the bottom topography is regionally important, because the TS is a key path for the exchange of water in the SCS with that in the ECS, the Yellow Sea and even the Sea of Japan [3-5].

Since 2009, the Taiwan Ocean Research Institute (TORI) of the National Applied Research Laboratories (NARLabs) has been providing consistent and accurate hourly surface current information in the seas around Taiwan. This is based on a significant effort to ensure hardware and software resiliency, quality control, and quality assurance. Spatial coverage of High Frequency radar (HF-radar), with a good data percentage of more than 50%, based on the past three years' records (see Figure 2), has been observed to vary on daily and seasonal scales due to ionospheric interference at the lower HF radio spectrum and variable state conditions. This coverage is uniquely capable of sampling relevant temporal and spatial scales of near shore processes that impact event response activities and basic coastal ocean research.

Remote sensing of near-surface currents with HF-radar was demonstrated more than 30years ago by Stewart and Joy. The measurement is based on the fact that electromagnetic radiation in the 3- to 30-MHz range scatters strongly (Bragg scattering) from ocean surface gravity waves. The returned energy spectrum thus indicates movement of ocean surface gravity waves with a wavelength of half the radar transmitted wavelength in directions either toward or away from the HF radar site (radial directions).Multiple radars are typically deployed so radials have enough angular separation to resolve both the north–south and east–west velocity components (hereafter referred to as totals). TORI employed the Seasonde technology which uses two directional antennas and a monopole antenna [6,7].

HF radar is a shore based remote sensing system, and is therefore subject to data gaps, which are predominately due to environmental effects, like increased external noise or low signal due to surface ocean conditions. Many applications of these surface current data require that these gaps be filled, including Lagrangian numerical models to estimate material transport and dispersion. The validation is based on observed surface current maps around the coast of Taiwan with specific common gap scenarios. Several techniques have been used to fill the gaps in the total vector maps. These are implemented using covariance made from normal mode analysis, open boundary modal analysis (OMA), Empirical Orthogonal Function (EOF) analysis, using idealized or smoothed

observed covariance and the recently developed, Least Square regression method based on the Discrete Cosine Transform (DCT-PLS) algorithm, which has been adapted to the mapping of hourly High Frequency Radar data observation [8-14].

The purpose of this study is to examine the usefulness of both High Frequency Radar data and Altimetry data in providing surface sub-mesoscale, mesoscale ocean circulation properties transport sand to improve our understanding of how physical processes influence coastal ecosystems. The rest of the paper is arranged as follows: Data sets are described in section 2; trajectory model and its evaluation methods are provided in section 3; regional results are reported in section 4, with a summary in section 5.

Data

The Lagrangian ocean observations were collected from Drifters trajectories, Altimetry product and High Frequency radars during May 2015 from measurements performed by the Taiwan Ocean Research Institute. The data points are reviewed in this section.

Drifter Trajectories

One drifter was released in the sea around Taiwan by the Taiwan Ocean Research Institute during the spring 2015 with the objective of providing a reference data set to validate trajectory predictions. The drifter was released within the coverage region of the national Taiwan CODAR system operated by TORI. The drifters were self-locating datum marker buoys (SLDMB). The drifter's location was recorded using a Global Positioning System (GPS) fixes at one hour intervals sampling and were transmitted to shore via the Argo communication, with a nominal GPS position uncertainty of 10m. Drifters were deployed in October 2015 both in the South China Sea (SCS) and in the Philippine Sea (PS).

As the drifter is rapidly advected northwards driven by the Kuroshio current after deployment and thus leaving the range of the HF radars, the results discussed in this section are limited to a single drifter experiment entrance to the TOROS domain, which started on 10 May 2015 at 00:00 UTC. Trajectories were run for 5 days. The skill score of data tracking was also evaluated by comparing observed and predicted trajectories. For this comparison, we used the method presented in which not only the end points of the observed and modeled trajectories were compared, but also the entire history of the drifter trajectories (3,6, and 9 hours' waypoints of the drifter trajectory) [1].

Altimetry Product

The Ocean Surface Current Analysis Real-time (OSCAR) offers gridded surface current data on global coverage, which allows us to extract surface current data in the TOROS domain. The OSCAR product, developed at Earth and Space Research (ESR), provides near real-time ocean surface velocities from satellite fields on global grid of 1/3 resolution with a 5-day interval [15-17]. The spatial coverage of OSCAR has been extended to as close to the coast as 1/3 degrees. This product is a direct computation of global surface currents using satellite SSH, scatter meter winds, and both Advanced Very High Resolution Radiometer (AVHRR) and in situ sea surface temperatures [18]. Currents are calculated using a quasi-steady geostrophic model together with an eddy viscosity based wind-driven a geostrophic component and a thermal wind adjustment. So, the OSCAR sea surface currents are averaged over the top 30 m of the upper ocean. The OSCAR data are also freely available through two data centers operated by NOAA and NASA JPL Physical Oceanography DAAC, respectively.

The High Frequency Radar Network

The Taiwan Ocean Radar Observing System (TOROS) of TORI consists of 17 SeaSonde type radars around the Taiwan Island (Figure 2), 12 of which are long range, 4 of which are medium range, and 1 of which is standard range. Table 1 provides the typical characteristics of the different types of systems. Each site consists of two categories of hardware: the radar equipment purchased directly from CODAR Ocean Sensors and the ancillary site specific hardware required for communications, power, backup power, temperature control, weather proofing, security, and antenna foundations. High Frequency Radar (HFR) systems are one technology deployed along the coast to remotely measure the complex surface current dynamics over these highly variable seas [19].

System Type	Radio Frequency (MHz)	Range (km)	Resolution (km)
Long Range	4.58	150	3.75
Medium Range	13.4	70	1.5
Standard Range	24.3	40	1.5

Table 1: Characteristic of Toros Long-, Medium-, and Standard Range Hf Radar Systems.

All of the sites are managed by Taiwan Ocean Research Institute (TORI), National Applied Research Laboratories (NARLabs) since 2009 and the primary function of the radars was to map surface currents. The TORI head

quarters in Kaohsiung processed all data, combined to surface current maps, checked for quality control, and saved to the archive. According to the 2014 TOROS annual report, the correlation coefficient of the surface current between HFR observed and 11 drifter-derived current velocities are 0.70 and 0.84 in u and v directions, respectively, and the mean differences are 0.019 m/s and -0.033 m/s in u and v directions [20].

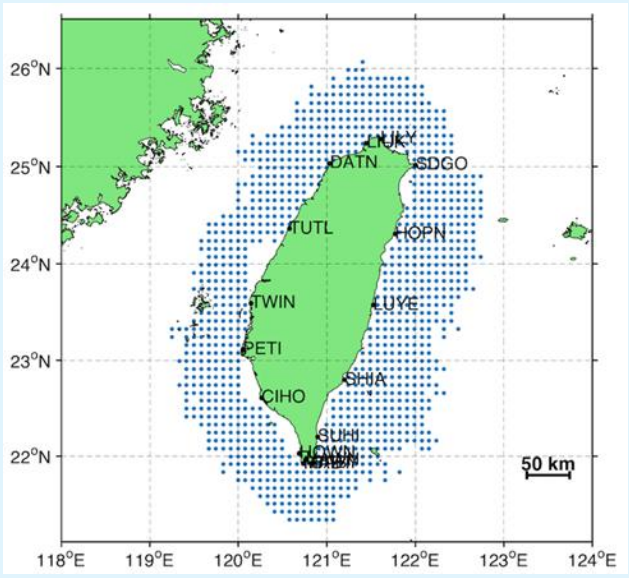

Figure 2: Location of long-range HF radar locations (black circle) within the TORI domain with four-letter site code next to station location overlay with the 70% mean coverage from May 01, 2015 to July 31, 2015 in seas around Taiwan.

The Gap Filling Method, Lagrangian Trajectory Model and Evaluation

The Gap Filling Method

Fredj et al. introduced for the first time a DCT-PLS method applied to HFR data processing. We now give a short introduction of the DCT-PLS algorithm. For more details on the mathematics of the method, the reader is referred to [14].

$$\boldsymbol{F}(\hat{X}) = RSS + sP = \left\| W^{1/2} \circ (X - \hat{X}) \right\|^2 + s\left\| \nabla^2 \hat{X} \right\|^2$$

Let X stand for a spatial-temporal dataset with gaps, and W a binary array of the same size indicating whether or not the values are missing. The technique consists in minimizing a criterion that balances the fidelity of the data, measured by the residual sum of squares (RSS), and a penalty term (P) that reflects the roughness of the smooth data $\hat{X}$ measured. The DCT-PLS seeks for an $\hat{X}$ that minimizes the error function. $\|.\|$ is the Euclidian norm, ∇^2 and $\circ$ stand for the Laplace operator and the Schur (element wise) product, respectively. The term s is a positive scalar that controls the degree of smoothing. As s increases, the smoothness of $\hat{X}$ also increases. For small values of s, the value of $\hat{X}$ will be dominated by noise. To investigate the best fit of the model coefficients, we apply the Generalized Cross Validation (GCV) score method to find a good compromise between goodness and smoothness of $\hat{X}$ [21]. In the case of equispaced data, simplified considerably the complexity of the GCV calculation by rewriting the GCV score in terms of the type-2 DCT and its inverse (IDCT), which forms [22]

$$\hat{X} = IDCT\left(\Gamma \circ DCT(W \circ (X - \hat{X}) + \hat{X})\right)$$

Where Γ are the components of the diagonal three-dimensional tensor defined by [23]

$$\Gamma_{i_1,i_2,i_3} = \left[1 + s\left(\sum_{j=1}^{3} (2 - 2\cos(i_j - 1)\,\pi/n_j)\right)^2\right]^{-1}$$

Where i_j denotes the i elements along the direction j, and n_j denotes the size of X along the direction j. The DCT-PLS technique relies only on the choice of the smoothing parameter s. In the case of gap filling the parameter s has an infinitesimal value to reduce the effect of smoothing. A high s value leads to the loss of high frequency variability in the HFR surface current fields. To avoid any subjectivity in the choice of the smoothing parameter, this parameter is determined by minimizing the GCV score. Minimization of the GCV score helps to optimize the trade-off between bias and variance. The bias measures how well the smoothed velocity field approximates the true velocity field, and the variance measures how well the smoothing velocity field can estimate the original experimental velocity field.

Lagrangian Trajectory Model: Lagrangian particle tracking is often found in oceanographic applications. A Lagrangian particle trajectory model, based on the surface velocity fields output from HF-radar corrected using our DCT-PLS algorithm. The Lagrangian trajectories of the "virtual" particles can be solved by the equation:

$$\frac{d\boldsymbol{r}}{dt} = \boldsymbol{u}(t, \boldsymbol{r})$$

Where $\boldsymbol{r} = (x, y)$ denotes the position of the particle and $\boldsymbol{u} = (u, v)$ is the Eulerian velocity at position $\boldsymbol{r}$ and time t. We hypothesize that the velocity of the particles is identical to that of the water (the virtual particles have no inertia and they do not interact with each other). The trajectories are evaluated using the Matlab Runge-Kutta 4/5th order to solve the Lagrangian trajectories. In addition, a linear interpolation in time and bilinear interpolation in space is performed due to the fact that the

temporal resolution of the velocity field is 30 minutes and the spatial resolution is 9km in the TORI network. Two measures will be used to quantify the trajectory hind cast to evaluate the relative performance of the HF-Radar TORIS: (1) the Lagrangian separation distance (d) , defined as the separation distance between the end points of the simulated and observed Lagrangian trajectories, and (2) a purely trajectory-based non-dimensional index (s) [1].

$$s = \begin{cases} 1 - \frac{c}{n}, (c \le n) \\ 0, \quad (c > n) \end{cases}$$

Following the suggestion of Lui, et. al., n is the tolerance threshold $n = 1$, and c is the normalized cumulativeLagrangian separation distance,

$$c = \sum_{i=1}^{N} d_i \Big/ \sum_{i=1}^{N} l_{oi}$$

Where $i = 1,2, \ldots, N$ and N is the total number of time steps, and d_i is the separation distance between the modeled and observed end points after the initialization of the virtual passive drifter, and l_{oi} is length of the observed trajectory. This definition is shown in the Figure (3). The smaller the s value, the worse the performance becomes, where s=0 implies no skill (the worst performance), and s=1 indicating a perfect fit between observation and simulation.

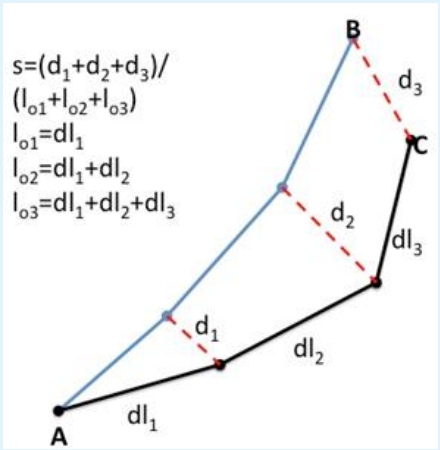

Figure 3: An illustration of the separation distances between the modeled and observed endpoints of Lagrangian trajectories (A-B and A-C, respectively) is shown in red. The lengths of the modeled (lm) and observed trajectories (lo) between the start and end points are shown in blue and in black, respectively. An index sis defined as an average of the separation distances weighted by the lengths of the observed trajectory.

Extended the non-dimensional skill score used for the skill score in the evaluation of a High Frequency Radar network to derive the performance.

Regional Results

This section focuses on evaluating the results of several measurements and demonstrating a hindcast system for the sub-mesoscale and mesoscale ocean circulation around Taiwan.

Dominant Current: The predominant wind system around Taiwan is the monsoon. The northeasterly monsoon prevails November–March, and the southwesterly monsoons prevail from May–September. April and October are transition months. The monsoon system is the primary force causing current variation around Taiwan [24]. Nitani described surface currents around Taiwan in summer and winter [25]. The Kuroshio flows to the north along the coast of Taiwan and the shelf break of the East China Sea Figure 1. In winter, the Kuroshio intrudes into the South China Sea in the Luzon Strait. In summer, water from the South China Sea enters the western edge of the Kuroshio [26]. East of Taiwan, the width of the Kuroshio is around 100 km, with a maximum speed of around 100cms^{-1}. The Kuroshio's pathway parallels the shoreline of Taiwan demonstrates no obvious seasonal variation Figure 1. South of Peng-Hu Archipelagos, current in the Taiwan Strait flows predominantly north-eastward regardless of the seasons. North of the Peng-Hu Archipelagos, the current flows north-eastward in summer and southwestward in winter. The seasonal variation is significant only in the Luzon Strait and in the northern Taiwan Strait. Many oceanographers believe that the Kuroshio intrudes into the South China Sea through the Luzon Strait in winter and stops in summer [24].

Gap-Filling Verification

The gap-filling algorithm was tested for two main scenarios observed in the hourly HFR current data in the seas around Taiwan. Based on the last three-month datasets (Figure 2), the gaps in the hourly maps around Taiwan are characterized with at least 70% spatial coverage, 70% of the time. In this study we defined two scenarios, which reproduce the most common gap situations (Figure 3).

Scenario 1: The first scenario mimicked a major hardware failure in July 9, 2015 14:00 with the loss of at least one site from the network. Observed gaps under this scenario extend along the coast from the shore to the offshore edge of the coverage, splitting the TORI HFR

network into two. The width of the gap across the coverage depends on the number of sites that are not reporting data. For this analysis, we are simulating the loss in contributing radials from a single site in HOPN region in the eastern part of Taiwan Island.

Scenario 2: The second scenario tested in June 2, 2015 16:00 mimics more common gaps in which each site is contributing radial vectors, but there is a reduction in the number of radial data from one or more sites. The most common cause of the reduced coverage is an increase in external noise that lowers the signal to noise ratio and therefore limits the range of detectable signal used to determine radial velocity. The size and location of the gaps depend on the location and magnitude of the reduction of coverage from each individual site. Forlong-range SeaSonde HF radar, the interference from the ionosphere effects can increase the noise floor, particularly at night. The impact of this ionospheric interference was observed on June 11, 2015 16:00:00 (Figure3).

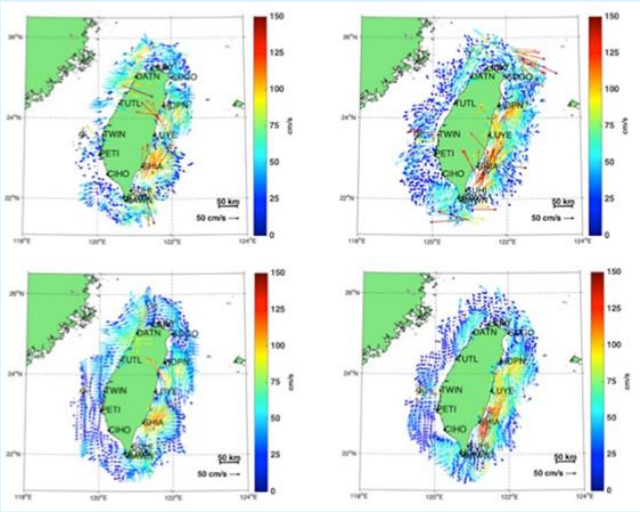

Figure 3: Surface current maps showing Scenario 1 on July 9, 2015 14:00:00 in the right column, and Scenario 2 on June 11, 2015 16:00:00 in the left column. The observed velocity field by TORI HFR is on the top and the smoothed velocity field map with 70% mean coverage is on the bottom.

Based on a 7-year analysis of TORI, from 2009 HFR coastal radar network, Scenario 1 occurs less than 6 % of the time and Scenario 2 occur almost 60 % of the time. For both Scenarios 1 and 2, we estimated the validity DCT-PLS velocity fields by comparing the removed vectors and the predicted vectors. The correlation shows a strong agreement between meridional and zonal velocity components.

Model Evaluation

The TOROS HF-Radars network validation is based on tracked drifter trajectories around Taiwan. For each drifter trajectory released daily at the observed location, and tracked using the HF-radars model network current velocities, both the Lagrangian separation distance d_9 and skill score s_9 are evaluated after 9 hours' simulations adapted from [1]. Figure 4 shows an example of simulated trajectories and the corresponding model skill scores s_9. A high skill score $s_9 \sim 0.8$ corresponding to better correlation between the simulated and observed trajectories is seen during 11-13 May 2015. The lower skill score $s_9 < 0.2$ is found for 10 May 2015 near the coast where the simulated particle diverges from the observed drifter trajectory. So, the skill score s_9 clearly indicates the poor performance of the TORI HF-Radars network.

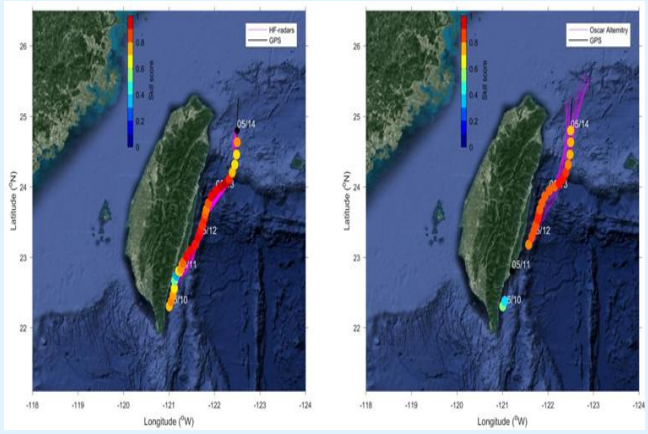

Figure 4: compares the simulated mean drifter trajectories initialized from the actual drifter # 1045 locations with the observed trajectories. The forecast skill score by TORI HF-radars and Oscar Altemitry is on the left and right, respectively. The drifter trajectory is represented by the black line and the predicted is colored red.

The Altimetry and HF-radars forecast skill score is highly dependent on the environmental conditions (see Figure 4). The complex flow structure was observed due to the strong Kuroshio current (~ 1 m/s) interacting with dramatically changed topography and the eddy transportation from the Pacific Ocean. HF-radars currents now cast provided the most valuable information for understanding of the coastal surface current, with a mean s_9 value of(0.4 – 0.7). In coastal zones (the strip of land within a few tens of kilometers from the coasts of Taiwan) the Oscar data is often contaminated by the land (see Figure 4 right panel in May 11, 2015), making the estimated velocity an extremely challenging task to

perform. The present research paves the way to confirm the reliability of TORI's HF-radars network.

The entire altimetry trajectories model has about the same performance, with mean s_9 value of (1 – 0.8) in the deep ocean and mean s_9 value of (0.6 – 0.7) within the transition zone from the shelf to deep ocean. Particularly within the transition zone from the shelf to the deep ocean, both the HF-Radars and Altimetry based trajectory models have reduced (20% – 30%)the skill score. Thus, comparisons focus mainly on the deep ocean region. Note that the OSCAR altimetry products skill score was not available near the coast, to avoid the problem of degraded performance of altimetry near the coast the comparison is restricted to buoys located in the open ocean no closer than 20 km to the coast.

Conclusions

In this study, we introduce an efficient automated DCT-PLS method for filling the data gaps in the HF-Radar ocean Spatial-Temporal dataset applied to TOROS domain in the seas around Taiwan. The DCT-PLS approach was demonstrated by reconstructing the hourly HF-Radar observation with a spatial resolution of nine kilometers across the Taiwanese seas. We validated the method during summer 2015 against typical gap scenarios. A major advantage of the approach is the ability to perform fast and robust computation while requiring a small amount of memory storage, demonstrating the feasibility of a real-time application for filling HF-Radar missing data. The user, however, should be aware of some limitations of the automatic gap filling procedure. Under the less common scenario in which more significant outages can remove entire sites from a coastal network, the effectiveness of the method depends on the characteristics of the surrounding flow. Individual HF-Radar network operators will need to assess the scales of variability in their operating area to determine the optimal way to apply this method in either a real-time or post-processed application.

This study has demonstrated a clearly higher skill score of surface data derived from HF-Radar than Oscar altimetry surface current in combination with drifter observations for offshore skill forecast. Furthermore, Oscar altimetry current surface achieves poor skill forecast in the offshore shell search area prediction. Surface currents derived based on both HF-radars and Altimetry affect the forecast skill score, especially in the region where the dramatic change of the bathymetry occurs alone the drifter trajectory. However, further investigation is required before concrete conclusions are made.

Acknowledgment

This study was supported by a grant from the Israel Science Foundation (ISF) and the Taiwan Ministry of Science and Technology. Taiwan Ocean Research Institute (TORI), National Applied Research Laboratories (NARLabs), sponsored the HFR dataset.

References

1. Liu Y, Robert H, Weisberg (2011) Evaluation of trajectory modeling in the different dynamic region using normalized cumulative Lagrangian separation, J Geophys Res 116(C9).

2. Liang W-D, Tang TY, Yang YJ, Ko MT, Chuang W-S (2003) Upper-ocean currents around Taiwan, Deep-Sea Research II 50(6-7): 1085-1105.

3. Jan S, Wang J, Chern C-S, Chao SY (2002) Seasonal variation of the circulation in the Taiwan Strait. J Mar Syst 35(3-4): 249-268.

4. Kondo M (1985) Oceanographic investigations of fishing grounds in the East China Sea and the Yellow Sea-I. Characteristics of the mean temperature and salinity distributions measured at 50 m and near the bottom. Bull Seikai Reg Fish Res Lab 62: 19-66.

5. Isobe A (1999) On the origin of the Tsushima warm current and its seasonality. Cont Shelf Res 19(1) 117-133.

6. Stewart RH, JW Joy (1974) HF radio measurements of surface currents. Deep-Sea Res 21(12): 1039-1049.

7. Barrick DE, BJ Lipa (1997) Evolution of bearing determination in HF current mapping radars, Oceanography 10(2): 72-75.

8. Lipphardt BL, Kirwan AD, Grosch CE, Lewis JK, Paduan JD (2000) Blending HF radar and model velocities in Monterey Bay through normal mode analysis. J Geophys Res 105 (C2): 3425-3450.

9. Kaplan DM, Lekein F (2007) Spatial interpolation and filtering of surface current data based on open-boundary modal analysis. J Geophys Res 112(C12).

10. Beckers JM, Rixen M (2003) EOF calculations and data filling from incomplete oceanographic data sets. JTECH 20(12): 1839-1856.

11. Alvera-Azcarate A, Barth A, Rixen M, Beckers JM (2005) Reconstruction of incomplete oceanographic

data sets using Empirical Orthogonal Fucntions: Application to the Adriatic Sea surface temperature. Ocean Modelling 9(4): 325-346.

12. Davis RE (1985) Objective mapping by least squares fitting. J Geophys Res 90(C3): 4773-4778.

13. Kim SY, Terrill E, Cornuelle B (2008) Mapping surface currents from HF radar radial velocity measurements using optimal interpolation. J Geophys Res 113(C10): 1-16.

14. Fredj E, Roarty H, Kohut J, Smith M, Gleen S (2016) Gap Filling of the Coastal ocean surface current from HFR data: Application to the Mid Atlantic Bight Network. JTECH 33: 1097-1111.

15. Lagerloef GSE, GT Mitchum, R Lukas, P Niiler (1999) Tropical Pacific near surface currents estimated from altimeter, wind and drifter data. J Geophys Res 104(C10): 23313-23326.

16. Johnson ES, F Bonjean, GSE Lagerloef, JT Gunn, GT Mitchum (2007) Validation and error analysis of OSCAR sea surface current, J Atmos Oceanic Technol 24: 688-701.

17. Dohan K, N Maximenko (2010) Monitoring ocean currents with satellite sensors. Oceanography 23(4): 94-103.

18. Bonjean F, GSE Lagerloef (2002) Diagnostic model and analysis of the surface currents in the Tropical Pacific Ocean. J Phys Oceanogr 32(10): 2938-2954.

19. Kohut J, Roarty H, Randall-Goodwin E, Glenn S, Lichtenwalner C (2012) Evaluation of two algorithms for a network of coastal HF radars in the Mid-Atlantic Bight. Ocean Dynam 62(6):953-968.

20. Lai JW, Lin KI, Yu CM, Hsu TC, Yang YC, et al. (2015) TOROS 2014 Annual Report. TORI Tech Note, p. 443.

21. Craven P, Wahba G (1978) Smoothing noisy data with spline functions. Estimating the correct degree of smoothing by the method of generalized cross-validation. Numer Math 31(4): 377-403.

22. Strang G (1999) The discrete cosine transform. SIAM Review 4(1): 135-147.

23. Yueh WC (2005) Eigenvalues of several tridiagonal matrices. Appl Math E-notes 5: 66-74.

24. Wirtky K (1961) Physical oceanography of the south east Asia waters. Scripps Institute of Oceanography NAGA Report 2: 195.

25. Nitani H (1972) Beginning of the Kurishio, In: Stommel H, Yoshida K (eds) Kurishio: Physical Aspects of the Japan Current. University of Washington Press, Seattle, pp. 441-500.

26. Zhang D, Lee TN, Johns WE, Liu C-T, Zantopp R (2001) The Kuroshio east of Taiwan: Modes of variability and relationship to interior ocean mesoscale eddies. J Physical Oceanography 31(4): 1054-1074.